Journal of Atmospheric and Solar-Terrestrial Physics 73 (2011) 40–51

Contents lists available at ScienceDirect

Journal of Atmospheric and Solar-Terrestrial Physics

journal homepage: www.elsevier.com/locate/jastp

Aspects of magnetopause/magnetosphere response to interplanetary discontinuities, and features of magnetopause Kelvin–Helmholtz waves

C.J. Farrugia [a,*], F.T. Gratton [b,c]

[a] Space Science Center, University of New Hampshire, Durham, NH 03824, USA
[b] Instituto de Física del Plasma, Consejo Nacional de Investigaciones Científicas y Técnicas, y Facultad de Ciencias Exactas y Naturales, Universidad de Buenos Aires, Ciudad Universitaria, 1428 Buenos Aires, Argentina
[c] Dep. de Física, Facultad de Ciencias Fisicomatemáticas e Ingeniería, Pontificia Universidad Católica Argentina, Buenos Aires, Argentina

ARTICLE INFO

Article history:
Accepted 18 October 2009
Available online 28 October 2009

Keywords:
Interplanetary discontinuities
Vortex sheets
Kelvin–Helmholtz instability

ABSTRACT

We describe (i) perturbations of the magnetopause/magnetosphere elicited by an interplanetary discontinuity and (ii) the production of Kelvin–Helmholtz waves on the magnetopause. These are two large topics, so for reasons of space we combine both features in a single data example, supporting the observations by theory. Correspondingly, the observations, made by ACE, consist of an interval in which a current sheet is followed by a period of strongly northward IMF. In view of recent attention directed at the effect of variations of the azimuthal component of the solar wind velocity on the magnetosphere, we chose a current sheet (CS) across which the east–west components of both field and flow vectors change polarity. A two-stage response is evident in the records of Cluster, outbound at the dusk terminator at 27° MLAT: (i) Four cycles of large-amplitude, ~3 min oscillations during which the spacecraft sample alternately the cold, dense magnetosheath and the hot and tenuous magnetosphere plasmas. We argue that these motions are likely due to tangential stresses applied to the magnetopause. (ii) Soon thereafter the oscillatory character changes dramatically, and ~80 s small-amplitude undulations appear which we argue to be magnetopause surface waves. Applying linear MHD theory we show these waves are due to a locally Kelvin–Helmholtz unstable boundary. As input parameters, we take values during the preceding large oscillations at the same magnetopause locale. An aspect of the non-linear phase of this instability is illustrated by a numerical simulation: the reduced duration of the evolution into large vortices by a strong initial perturbation.

1. Introduction

Directional discontinuities (DD) are common in the solar wind. Their effects on the magnetosphere magnetic field and plasma populations have been the subject of much study over the years. The arrival of the pressure increase associated with the interplanetary shock driven by an interplanetary coronal mass ejection (ICME) or a magnetic cloud is well known to compress the low-latitude geomagnetic field through an intensification of the Chapman–Ferraro magnetopause (MP) current, leading to a so-called "sudden impulse (SI)" in low-latitude magnetometer records. The SI is a good time marker of possibly much stronger disturbances to follow during the passage of the ICME-sheath and the ICME itself. An early thrust concerned the ionospheric signatures of flux transfer events (FTEs), characteristic signatures at the MP ascribed to sporadic bursts of reconnection (Russell and Elphic, 1978). Models for the current system (Saunders et al., 1984; Southwood, 1987; McHenry and Clauer, 1987, see correction McHenry and Clauer, 1989) were elaborated. Yet, it was also soon realized that similar magnetic deflections could be caused by MP motions driven by changes in the external pressure (Farrugia et al., 1989; Freeman et al., 1990; Sibeck, 1990). Thus, to help distinguish between the two sources, the suggestion was made to use chains of ground stations rather than depend on the records from a single station.

Traveling convection vortices and magnetic impulse events (Friis-Christensen et al., 1987) are convection disturbances ascribed to the dynamic pressure changes which often accompany DDs. As implied by these works, aside from sharp rotations in the magnetic field (for example, from north to south), which can drastically alter the coupling of solar wind mass and momentum at the MP, the dynamic pressure plays a major role in exciting important MP motions and various types of oscillations in the magnetospheric cavity.

To understand fully the effects on the magnetosphere of pressure changes associated with DDs one must not forget the bow shock. Significant advances in our understanding of this aspect were achieved through numerical simulations, most

* Corresponding author.
E-mail address: charlie.farrugia@unh.edu (C.J. Farrugia).

1364-6826/$ - see front matter © 2009 Elsevier Ltd. All rights reserved.
doi:10.1016/j.jastp.2009.10.008

notably those of Wu et al. (1993). These authors simulated the arrival at the bow shock of a tangential discontinuity (TD) and noted that, when the density across the TD changes, subsidiary MHD modes (fast mode waves, slow rarefaction waves, and the [altered] TD) are generated when the original TD interacts with the bow shock. The MP would react first to the fast-mode wave which, though it carries only a fraction of the initial density change, travels ahead of the TD. Recent works showing experimentally the presence of the fast mode wave (or rarefaction wave, if the density decreases) and TD in the magnetosheath produced by this TD-bow shock interaction are those of Fairfield et al. (2003) and Maynard et al. (2008). The reader's attention is also directed to the extensive numerical simulations undertaken by Lin and co-workers addressing the interaction with the bow shock of pressure pulses and variations in the IMF direction, including DDs (Lin, 1997; Lin et al., 1996a, 1996b; Cable and Lin, 1998). Clearly, the wave modes produced at the bow shock need to be borne in mind when studying the magnetosphere response.

Compared to the changes in dynamic pressure, which involve the density and the flow velocity normal to the DD plane, much less attention has been directed to the changes in the solar wind azimuthal flow direction which might occur at the DD. These contribute to the off-diagonal elements of the total pressure tensor (momentum flux tensor). In a remarkable departure, Zong et al. (2004) studied the motions of the dayside cusps and found a large response which they concluded was temporal, and which they attributed to just these velocity changes. Earlier work by Lundin et al. (2001) had also highlighted the potential importance of these changes to the cusp.

Given that the magnetized solar wind flows around the magnetosphere, and keeping in mind the velocity shear that thus exists at the MP boundary, a lot of effort has been devoted to the possibility of exciting Kelvin–Helmholtz waves at the MP surface when, in addition, the IMF is northward-pointing, starting with the seminal work of Dungey (1954). This is particularly so near the flanks, where the speed approaches and exceeds the sonic limit. In magnetospheric physics, computational Kelvin–Helmholtz investigations began with the pioneer work of Miura (1984, 1987, 1990). Many observational and numerical simulation studies have been conducted (see e.g. reviews by Belmont and Chanteur, 1989; Kivelson and Chen, 1995; Farrugia et al., 2001). Studies on KH activity at the dayside MP, too, revealed many interesting features (Farrugia et al., 1998; Gratton et al., 2004). The situation at the MP is complicated by two factors: (i) the magnetized nature of the flow around a magnetized planetary environment, because of the need to overcome restraining magnetic forces for the waves to grow, and, particularly down the flanks, (ii) the effect of compressibility, which is generally stabilizing.

In this select review, we study the effect of an interplanetary CS downstream of which the magnetic field turned strongly northward. Some aspects of the scenarios outlined above will be at the forefront: (i) the changes in the tangential stresses are stronger than the normal stress, so any oscillatory behavior of the MP will have these as their primary cause. The small dynamic pressure change was associated with only a small density change across the CS, so that the complications arising at the bow shock (which are a strong function of the density change, Wu et al., 1993) are much attenuated, and the CS is essentially pristine when it impacts the MP. We shall then apply compressible MHD calculations to show that the subsequent northward IMF interval ushered in a period when the MP was KH-unstable. We shall use data from ACE and Cluster. The two-step trigger resulted in a two-stage response at the duskside MP monitored by Cluster: first, ~ 3 min, large-amplitude oscillations were set up, and later (ii) small-amplitude, higher frequency (~ 12.5 mHz) oscillations were visible. We shall capitalize on the favorable circumstances by using as input values to the KH calculations extreme values attained during the previous large-amplitude oscillations, eliminating thereby one common source of error in such studies (namely, boundary conditions measured far away in time). We end with a brief description of one aspect of the non-linear MHD calculations, namely, the appearance of large vortices.

2. ACE observations

The interplanetary observations are from the ACE spacecraft, in orbit around the L1 Lagrangian point and located at $(228, 40, -9)$ R_E (Earth radii; GSE coordinates) during the interval of interest (~ 13 UT). For the 1-h period 12:30–13:30 UT, Fig. 1 displays the solar wind density, bulk flow speed, dynamic pressure, total pressure (thermal + magnetic pressures), total field strength, the east–west components of the magnetic field and flow vectors, and the IMF clock angle (i.e. the polar angle in the GSM YZ plane). The data are from the SWEPAM (plasma; McComas et al., 1998) and MAG (Smith et al., 1998) instruments and are plotted at 64 s and 16 s resolution, respectively, in the GSM coordinate system. A field and flow discontinuity passes ACE at 12:47 UT (vertical guideline). Highlighted by arrows are two strong changes which occur in the east–west components of the field (B_y) and the flow (v_y) vectors, both of which rotate from west to east. Further, at the DD, the magnetic field assumes a northward orientation. Taking 5-min averages on either side of the DD, we find that the density (first panel) undergoes only a small change which, together with a similar small change in bulk flow speed, results in only a $\sim 17\%$ increase in the dynamic pressure. During the $\sim 16-$min period 12:55–13:11 UT shown by the thick trace in the bottom panel the IMF clock angle is low. The 30-min interval $\sim 12:45-13:15$ UT is the one whose effect at Cluster we shall examine.

We used 1 s resolution data to carry out a minimum variance analysis (Sonnerup and Cahill, 1967) on the ACE magnetic field data for five nested intervals around the DD. In each case a reliable normal could be determined and the angular spread of the normals was of order 10°. A representative normal is $\mathbf{k} \equiv \mathbf{n} = (-0.86, -0.38, 0.34)$ (GSM), i.e. pointing antisunward, dawnward and southward. Further, in all cases the normal component of the magnetic field was consistent with zero. The DD thus satisfies a necessary condition for being a tangential discontinuity. However, a firm conclusion cannot be drawn for the following reason. The interval 12–14 UT at ACE is marked by clear Alfvénic fluctuations. (The correlation coefficients for the individual field and flow components are 0.64(x); 0.88(y) and 0.86(z)). As shown by Vasquez et al. (2007), a statistically likely physical alternative is a CS generated by turbulence. This too has a small normal component, consistent with the strong perpendicular energy cascade typical of Alfvénic turbulence. Henceforth we shall consider this DD to be a combination of a CS with a VS.

3. GOES 8 and Cluster observations

We show first in Fig. 2 the measurements made by NOAA's GOES 8 geostationary satellite in the period 13:45–15:00 UT, covering the $\sim 10-11$ magnetic local time (MLT) range. The data are in spacecraft coordinates (P, E, N), where P is orthogonal to the spacecraft's orbital plane (approximately parallel to the Earth's spin axis), E is perpendicular to P and points earthward, and N is perpendicular to P and E and is directed eastward. The data are at 0.5 s time resolution. Our focus is on the profile of the total field, which undergoes a compression at $\sim 13:57$ UT. This compression,

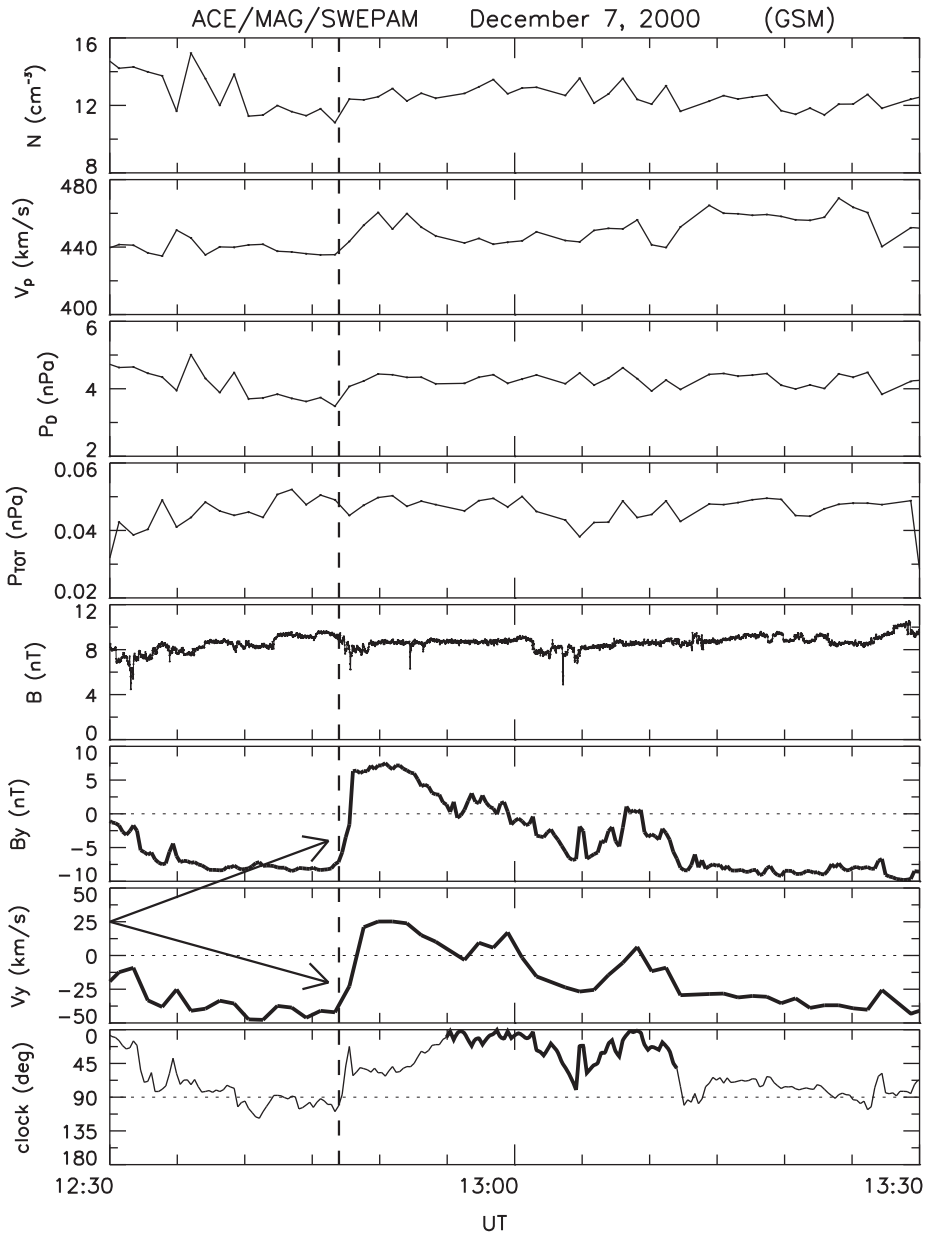

Fig. 1. ACE plasma and magnetic field data. From top to bottom: the proton density, bulk speed, dynamic pressure and total pressure (plasma+field), the magnetic field strength, the east–west components of the magnetic field and flow vectors and the IMF clock angle, i.e. the polar angle in the GSM (*YZ*) plane. Arrows mark the DD, and the heavy trace in the last panel indicates the interval of strongly northward IMF following the DD.

which is much like an SI, marks the time when information on the normal and tangential stresses at the MP reach the GOES 8 spacecraft via fast magnetosonic waves propagating within the cavity. At around this time, ground magnetometer stations from arrays spread ~ 12 h in MLT record a transition to large, coherent oscillations (see Farrugia et al., 2008a, for further details). We may thus use the SI at GOES 8 as a timer, and conclude that the ACE-ground delay is ≈ 70 min.

On December 7, 2000, the Cluster spacecraft were on an outbound trajectory and, between 12–17 UT, they was just tailward of the dusk terminator ($X \approx -2R_E$; $Y \approx 12R_E$, 18.1 MLT) at northerly magnetic latitudes (26° MLAT). Fig. 3 displays in the top panel the radial distance R_{CL} of Clusters 3 and 4 (dashed) relative to that of the model MP of Shue et al. (1998) (R_S, jagged trace). The latter, which includes the two major interplanetary parameters affecting the position of the MP, i.e. IMF B_z and solar wind P_{dyn}, is computed from the ACE data time-shifted by the estimated 70 min. The time of interest to us is marked by the thick horizontal bar. It is seen that during this time the spacecraft were according to the model in the environs of the MP and its boundary layer, an inference which is confirmed by the data discussed shortly. The bottom panel shows the position coordinates of Cluster 4 in the GSE system.

One may obtain the impact point of the CS/VS as follows. One assumes that the (planar) CS passes unaltered through the bow shock. Further, the Shue et al. (1998) model gives the distance of the subsolar MP ($\sim 9.2R_E$) for the prevailing average solar wind pressure (~ 4 nPa), and the shape factor of the magnetosphere, i.e. the ratio of the distance to the terminator and the distance to the subsolar point ($= 1.56$, not shown). It can then be shown that the impact occurs at $(7.2, 5.0, -4.4)$ R_E, i.e. at mid-afternoon MLTs and at southerly latitudes.

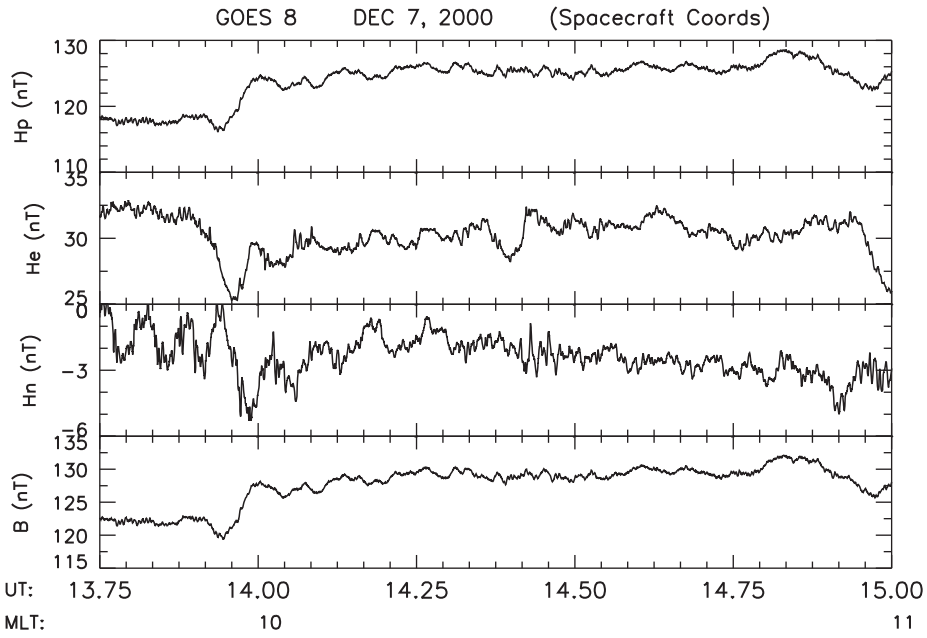

Fig. 2. Magnetic field data from NOAA's GOES 8 spacecraft in the ~10−11 MLT sector. The data are in spacecraft coordinates (see text). Note the increase in the field strength at ~13 : 57 UT.

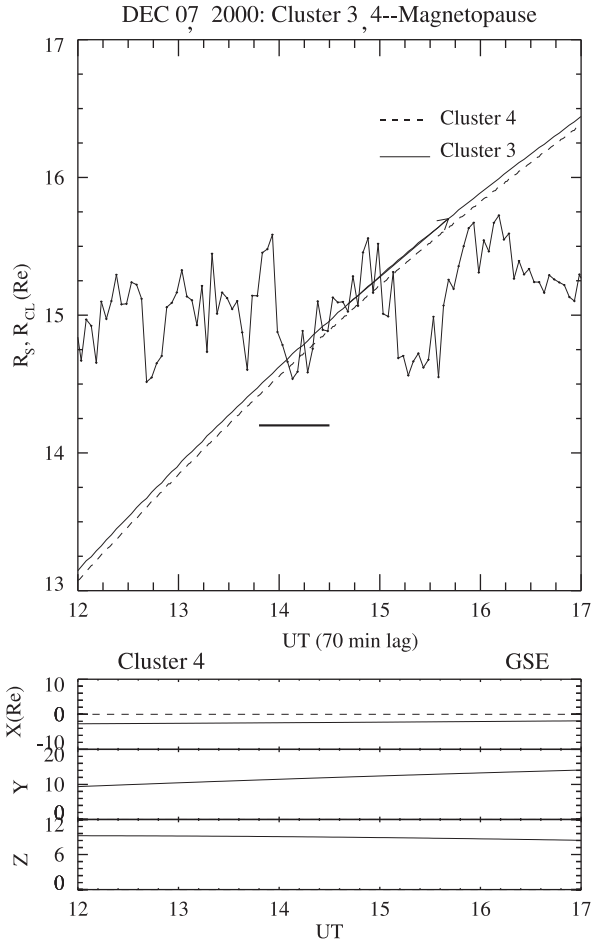

Fig. 3. The radial distance of Clusters 3 and 4 from the model magnetopause of Shue et al. (1998). The time interval we are interested in is shown by a thick horizontal bar. The bottom panel shows the position coordinates of Cluster 4 (GSE coordinates).

Fig. 4 shows Cluster 3 plasma and magnetic field data in GSM coordinates from the CIS (Rème et al., 1997) and FGM (Balogh et al., 1997) instruments during the 40-min interval 13:54 UT–14:30 UT. The data are plotted at spin average (~4 s) resolution. From top to bottom, the figure shows the proton density, temperature, and bulk speed, the total field, and the GSM components of the field and flow vectors. From the character of the fluctuations one can distinguish two contiguous phases, delimited by the vertical guidelines. In the first (marked I in panel 2) lasting from 13:58 UT to 14:10 UT, large-amplitude oscillations in various quantities are evident, most notably in the density, temperature and bulk flow speed. Four cycles may be identified, yielding an average period of 3 min. A hot ($T_p \leq 6 \times 10^7$ K), tenuous ($N \sim 2\,\mathrm{cm}^{-3}$), and slow or stagnant ($V \leq 50\,\mathrm{km\,s}^{-1}$) proton plasma alternates with one which is cold ($T_p \leq 5 \times 10^6$ K), dense ($N \geq 12\,\mathrm{cm}^{-3}$) and fast ($V \geq 100\,\mathrm{km\,s}^{-1}$). These oscillations set in when the effects of the tangential stresses on the MP arrive at the spacecraft location. It appears that the MP is oscillating bodily over the spacecraft.

It is a familiar notion that the arrival of a spatially non-uniform pressure perturbation creases the magnetopause. In the present case, the sudden application of a spatially non-uniform shear stress generates similar wrinkles on a deformable boundary. The oscillations are determined by the properties of the magnetopause and its surroundings, as in the motion of a pendulum.

These large oscillations then die out, only to be replaced in the second phase (14 : 10 UTto~ 14 : 26 UT) by another type of oscillation, most evident in the field and flow components and the total field and flow (marked II in panel 2).

To examine the large oscillations further, Fig. 5 shows proton spectrograms for Cluster 3 (top) and Cluster 4. Proton energy differential fluxes are plotted. It appears that during the 3 min-period, large-amplitude oscillations, CIS records the alternate presence of high and low energy protons. We shall assume that at the extremes of the oscillations the spacecraft sample the magnetosphere and the magnetosheath plasmas, respectively. Later, during the higher frequency oscillations, the low energy

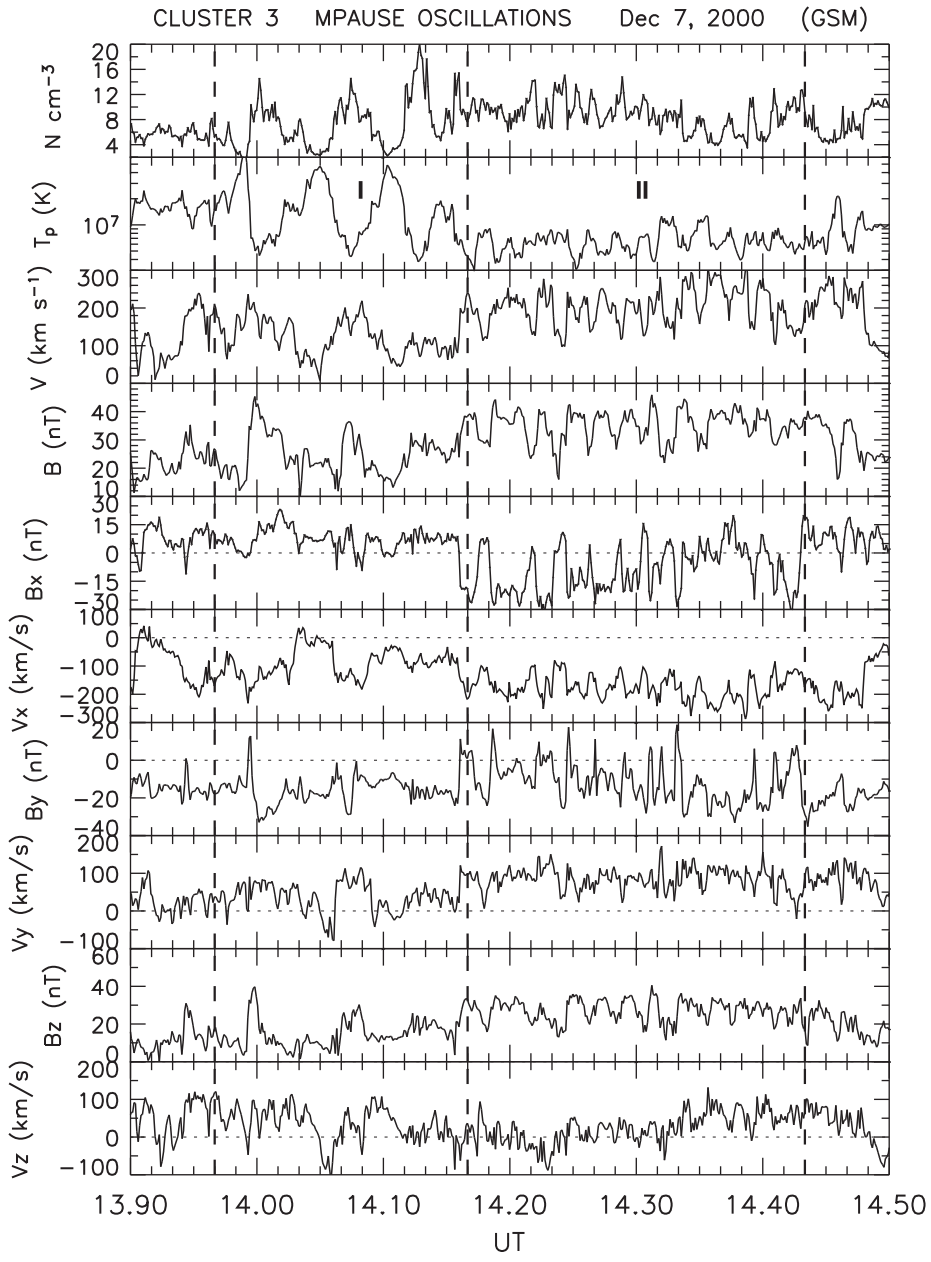

Fig. 4. Proton plasma and magnetic field measurements made by Cluster 3 from 13:54 to 14:30 UT. From top to bottom are shown the proton density, temperature and bulk speed, the total field, and (pairwise) the field and flow components (in GSM coordinates). Vertical guidelines bracket the two intervals where different oscillatory behavior was in evidence.

population is always present but the high energy component is episodically depleted, i.e. the oscillations are in the high energy component. We interpret this in terms of an MP wave sweeping past the spacecraft which goes alternately into the sheath (only low energy particles present) and the boundary layer (both high and low energies present).

Fig. 6 shows the power spectral density of the B_z component of the magnetic field at Cluster 3 for the time interval 14:09–14:26 UT (phase II). To obtain the fluctuations, an average over the whole interval was subtracted. A spectral peak is evident at ~ 12.5 mHz, corresponding to a period of 79.4 s. This frequency lies in the Pc-4 range, an oft-quoted range in which micropulsations are excited in the magnetosphere as field line resonances due to KH instability. Below we shall examine this hypothesis further.

4. Interpretation

4.1. The total pressure tensor

We discuss first the cause of the large-amplitude waves. Motivated by the work of Zong et al. (2004), we shall evaluate the elements of the total pressure tensor (momentum flux tensor), given by

$$\Pi_{\alpha\beta} = \left(p + \frac{B^2}{2\mu_0}\right)\delta_{\alpha\beta} + \rho V_\alpha V_\beta - \frac{B_\alpha B_\beta}{\mu_0},$$

where α, β are running indices (i, j, k). Using the CS/VS coordinates i, j, k with $B_k = 0$, the component of pressure tensor normal to the

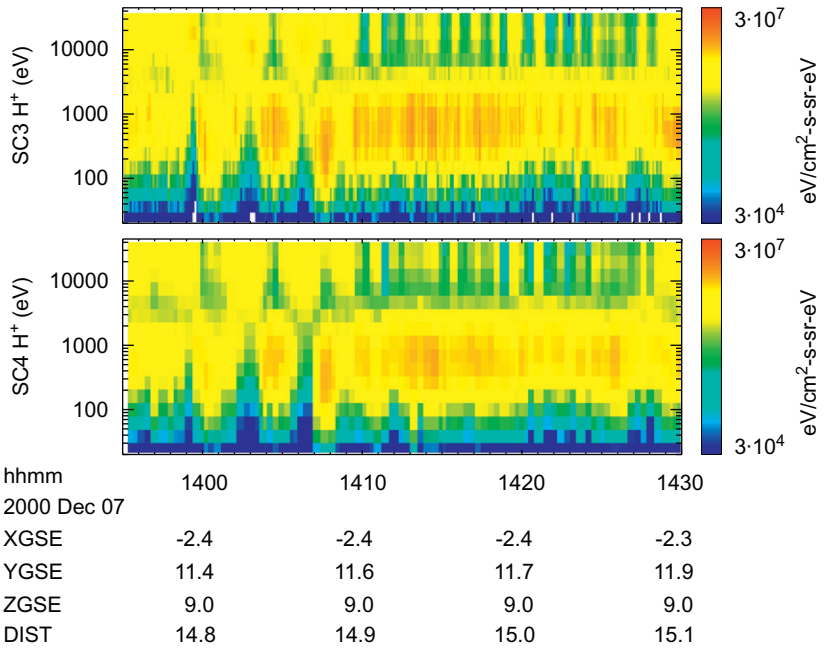

Fig. 5. Proton differential fluxes (color coded) from Clusters 3 (top) and 4 for the time interval 13:50–14:30 UT. (For interpretation of the references to color in this figure legend, the reader is referred to the web version of this article.)

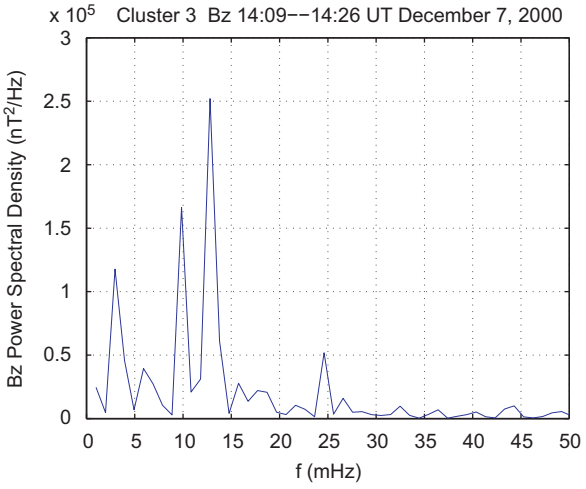

Fig. 6. Power spectral density of B_z (Cluster 3) for the period 14:09–14:26 UT. An average over the whole interval has been subtracted.

discontinuity plane is

$$\Pi_{kk} = \rho V_k^2 + p + \frac{(B_i^2 + B_j^2)}{2\mu_0}.$$

Note that at the moment of impact, vector **k** is normal to both the discontinuity as well as the MP, so that this expression represents the pressure normal to the MP boundary. The components of the pressure tensor along the CS/VS plane are

$$\Pi_{k\beta} = \rho V_k V_\beta,$$

where $\beta = i, j$.

Fig. 7 displays in the first panel the normal components Π_{kk} (dashed) and $P_{kk}(=\rho V_k^2)$, from which it is immediately clear that the magnetic contribution is negligible. The second and third panels show the stresses tangential to the MP. We average over 5 min on both sides of the DD and we find that the change in the tangential stresses $([(\Delta\Pi_{ki})^2 + (\Delta\Pi_{kj})^2]^{1/2})$ is about three times that of the normal pressure ($\Delta\Pi_{kk}$; 0.55 nPa vs. 0.18 nPa). We thus conclude that it is these tangential stresses which are the main cause of the large deformations of the MP in the earlier phase of the event and which were seen by Cluster as 3 min-period oscillations of the whole boundary over the spacecraft.

4.2. KH instability: application of linear theory

The higher frequency oscillations occur when the field is northward pointing (Fig. 1). We now examine the hypothesis that these are MP waves which were excited by the Kelvin–Helmholtz instability.

The local stability of the flanks of the MP is governed in MHD theory by two main parameters, the sonic Mach number $M_s = U_1/c_s$, and the Alfvén Mach number $M_A = U_1/V_A$, where U_1 is the flow velocity, c_s is the speed of sound, and V_A denotes the Alfvén velocity, all quantities being evaluated at the adjacent magnetosheath (see also Miura, 1990, 1992). In addition, a key factor is the existence of magnetic shear across the boundary, which may prevent the development of the instability. Both parameters M_s and M_A increase toward the MP tail. The presence and relevance of magnetic shear at the near flank depend on the interplanetary conditions.

Plasma compressibility may also exert a considerable influence on the stability of a velocity shear flow when the velocity difference $\Delta\mathbf{V}$ across the gradient layer is supersonic (González and Gratton, 1994a, 1994b). However, in the event considered here, $M_s \lesssim 1$ at the Cluster crossing site and therefore, although the theory takes compressibility into account, the latter is not a strong effect. In any case, the non-uniform density of the transition layer, the presence of magnetic shear across the boundary, and plasma compressibility (when M_s is comparable to, or larger than, unity) are the principal properties that a stability analysis must consider (Gratton et al., 1988).

For long-wavelength waves the MP can be considered locally as a tangential discontinuity (TD). The question of the Kelvin–Helmholtz (KH) stability of the MP, however, is more complex than what is revealed by a TD approximation because it depends

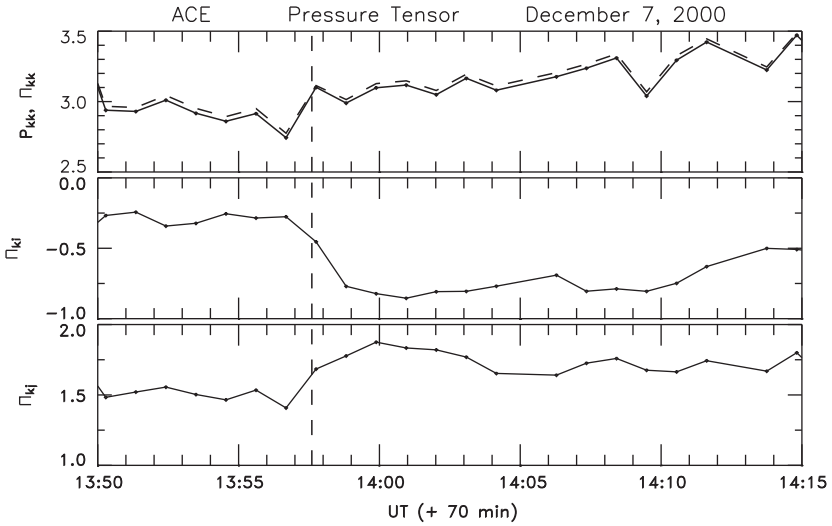

Fig. 7. Elements of the total pressure tensor. The top panel shows the normal component, with (dashed), and without, the magnetic field contribution. There follow the stresses tangential to the boundary in the i th and j th directions, respectively. (Reproduced by permission.)

on several other elements not considered in that simple model. The ratio λ/Δ of the mode wavelength ($\lambda = 2\pi/|\mathbf{k}|$) to the width Δ of the boundary layer is important because a TD model (where $\Delta \to 0$) may be stable while a finite-Δ theory shows instability (Gratton et al., 2004, 2005).

An important feature of the MP both on the flanks as well as on the frontside is the presence of the low latitude boundary layer (LLBL), a region whose physical values are intermediate between those of the magnetosheath and the magnetosphere proper. The flow velocity decreases across the boundary layer without changing its antisunward direction (except occasionally when a weak counterflow may appear in the magnetosphere). The instability mechanism can feed better at the LLBL when the magnetic shear is small, because in that case the magnetic tensions can be switched-off by perturbations having $B_\kappa = \mathbf{B}\cdot\boldsymbol{\kappa} \approx 0$, known as *flute* modes. Moreover, inside the LLBL the plasma flow is subsonic since the speed has decreased, while the sound velocity has increased, with respect to magnetosheath values. The latter effect is due to the strong temperature enhancement as the magnetospheric plasma is approached. Conversely, the stabilizing influence of compressibility is expected to be more effective at the MP interface.

Numerical work on the linear stability of finite-Δ models of the boundary layer is based on a compact second order differential equation of the KH modes given in Gratton et al. (1988). The boundary layer model is built with continuous functions for the main physical quantities. The theory is an ideal (non-resistive), compressible, MHD treatment, sufficient to elucidate the experimental issues discussed in the paper. The boundary value problem that provides the growth rate, and other properties, of the unstable modes is solved numerically.

The December 7, 2000, event corresponds to a period in which the IMF has a dominant northward component. This interplanetary condition is the most favorable for the KH instability at the near equatorial flanks, since the interplanetary magnetic field lines tend to be aligned with the geomagnetic field lines, thus reducing the magnetic shear across the boundary. Vortices generated by the KH instability at the boundary layer become important agents of momentum, energy transfer from the solar wind to the magnetosphere. We also briefly discuss the build-up of vortices as a consequence of the KH development, commenting on some results of a non-linear numerical MHD simulation (Gratton et al., 2009).

We carried out a linear perturbation analysis of the compressible, ideal MHD equations. We use a stratified model of the boundary layer with physical quantities varying as hyperbolic tangents across the layer, joining in a continuous way the quantities on either side. For the magnetosheath and magnetosphere input conditions we use values measured by Cluster 4 at the extremes of the second large oscillation, from $\sim 14:03$ to 14:05 UT. The main parameters are listed as follows:

14 : 05 UT	*Magnetosheath*	14 : 03 UT	*Magnetosphere*
n_1 (cm^{-3})	13.6	n_2 (cm^{-3})	2.3
B_1 (nT)	34.6	B_2 (nT)	22.1
U_1 (km s^{-1})	139	U_2 (km s^{-1})	~ 0
T_1 (keV)	0.38	T_2 (keV)	~ 2.6
$\angle \mathbf{B}_1\mathbf{V} = \theta_1$	121°	$\angle \mathbf{B}_2\mathbf{V} = \theta_2$	126°

From these values it follows that at the Cluster position the sonic Mach number $M_s = 0.57$, and the Alfvén Mach number $M_A = 0.70$. The magnetic shear angle $\delta\theta \equiv \theta_2 - \theta_1$ (i.e. the change in direction of the magnetic field lines from one side to the other) is very small $\sim 5°$, i.e. the field lines are nearly aligned.

We work in a local coordinate system in which the boundary layer extends in the y-direction, positive pointing to the magnetosheath. Physical quantities are constant over $y =$ constant planes, i.e. they depend only on y. The x coordinate is along the mean bulk velocity vector (antisunward), z completes a right-handed Cartesian coordinate triad. The MHD perturbation of the boundary layer is described by Fourier modes of the form

$$\Xi = \zeta(y)\exp(-i\omega t + ik_x x + ik_z z), \tag{1}$$

where Ξ is the y component of a plasma element displacement from equilibrium. The amplitude of the shift is denoted by $\zeta(y)$. Quantities $k_x(k_z)$ are the x (z) components of the wavevector and $\omega = \omega_r + i\gamma$ is the (complex) frequency. As derived elsewhere (Gratton et al., 1988), the MHD stability equation is

$$\frac{d}{dy}\left[H\left(1-\frac{1}{M}\right)\frac{d\zeta}{dy}\right] - k^2 H\zeta = 0, \tag{2}$$

where the functions H and M are defined by

$$H(y) = \rho(y)(c - V_\kappa(y))^2 - B_\kappa^2(y)/4\pi, \tag{3}$$

$$M(y) = 1 - \frac{(V_A^2 + c_s^2)}{(c - V_\kappa)^2} + \frac{(V_{A\kappa}^2 c_s^2)}{(c - V_\kappa)^4}. \tag{4}$$

In these expressions V_κ and $V_{A\kappa}$ are the projections of **V** (flow velocity) and $\mathbf{V}_A = \mathbf{B}/\sqrt{4\pi\rho}$ on **k**, respectively. Function H contains two terms, the first of which drives the instability (via the projection of **V** on the wave vector **k**) and the second is the restoring magnetic tension force (with a similar projection B_κ). The function M contains the effects of compressibility. It is relevant mainly when the flow velocity becomes comparable to, or larger than, the sound speed. The limit $c_s \to \infty$, for which $M \to \infty$, corresponds to the incompressible regime.

The characteristic value $c = \omega/k$ (complex phase velocity) is the main unknown of the boundary value problem. It is a function of the velocity, magnetic field and density profiles across the boundary layer. Fig. 8 shows the most important functions of the analysis for December 7, 2000, the components of velocity V_k and magnetic field B_k for the most unstable **k**–vector direction. This occurs at an angle of $+32^\circ$ to the main flow, which produces minimum magnetic shear across the layer. The minimum is reflected in the small values of B_k. The right-hand axis (with a very short range -2 to 1.2 nT) refers to B_k. The left-hand axis (with range 0-120 km/s) is for V_k.

The normal modes must tend to zero on either side of the MP, that is, $\zeta \to 0$ when $y \to \pm\infty$. However, for a given **k**, this happens only for particular values of the complex frequency. The boundary value problem c is solved numerically by a conventional shooting method (see, for instance, Keller, 1992).

Fig. 9 shows the resulting change of the growth rate, γ, of the unstable modes, normalized as $\gamma d/U_1$, vs. the absolute value of the normalized wave number kd. Both quantities are expressed in dimensionless numbers using parameter $d = \Delta/2$, where Δ is the width of the LLBL, and U_1 is the plasma velocity of the magnetosheath close to the MP. The results are shown for a particular angle between **k** and **V**, i.e. $\phi = 32^\circ$, the angle that gives the maximum growth rate. This angle is found by varying the orientation of **k** in the (x,z) plane. For this angle, the **k**–direction is almost perpendicular to both, inner and outer magnetic fields. Thus, the magnetic tensions are minimized and their stabilizing action removed (*flute modes*). The maximum growth rate is given by $\gamma_m = 0.079\ U_1/d$ for a mode with wavenumber $k_m d = 0.55$. Modes with other **k**–directions have smaller growths (see Fig. 10). The figure is drawn from numerical results of the boundary value problem for the modes. The KH stabilization at short wavelengths ($kd = 1.2$) is typical of studies with continuous profiles. It stems from the limited extent of the modes in the y-direction which

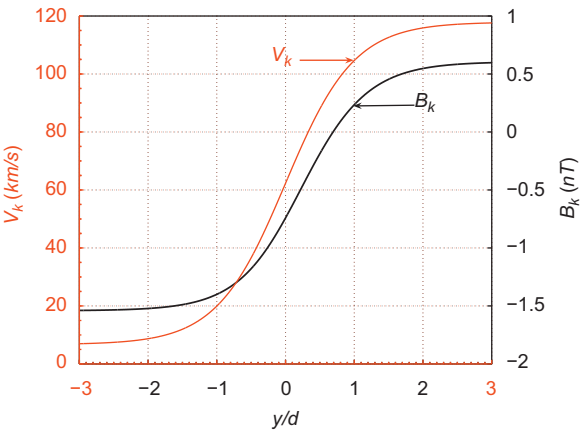

Fig. 8. Components of velocity V_k and magnetic field B_k along the direction of the **k**–vector of the mode. These functions have a principal role in the differential equation of the KH instability. The **k**–vector is at an angle of $+32^\circ$ to the main flow, a direction which gives minimum magnetic shear across the boundary layer and, correspondingly, maximum growth of the instability. The left-hand axis is for V_k and the right-hand axis is for B_k.

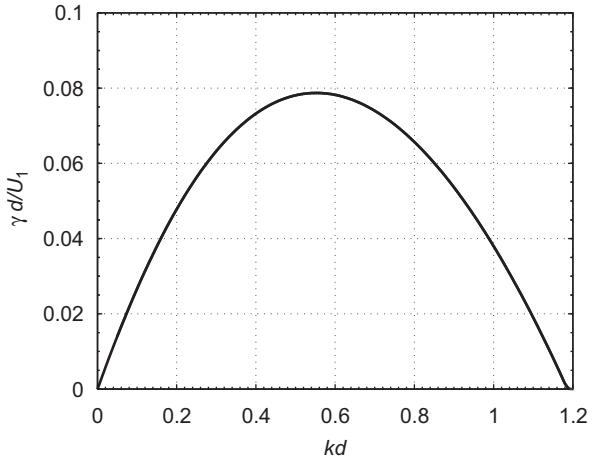

Fig. 9. The growth rate γ of the KH instability as a function of the wavenumber k. The imaginary part of the characteristic value c is related to $\gamma = Im(kc)$. The modes grow as $\exp(\gamma t)$ during the linear stage of the process. The plot is for a fixed orientation of the **k**–vector, inclined $+32^\circ$ to the main flow (antisunward direction). This angle gives the maximum growth rate (achieved for $kd = 0.55$). The maximum is at $\gamma d/U_1 = 0.079$. Modes with other **k**–directions have smaller growths (see next figure). Growth rates are normalized with U_1/d, and the wavenumbers with $1/d$. Here U_1 is the velocity in the adjacent magnetosheath, and $2d = \Delta$ is the scale length of the velocity gradient, which is indicative of the thickness of the boundary layer. The figure is drawn from numerical results of the characteristic boundary problem for the modes. The KH stabilization at short wavelengths ($kd = 1.2$) is typical of studies with continuous profiles.

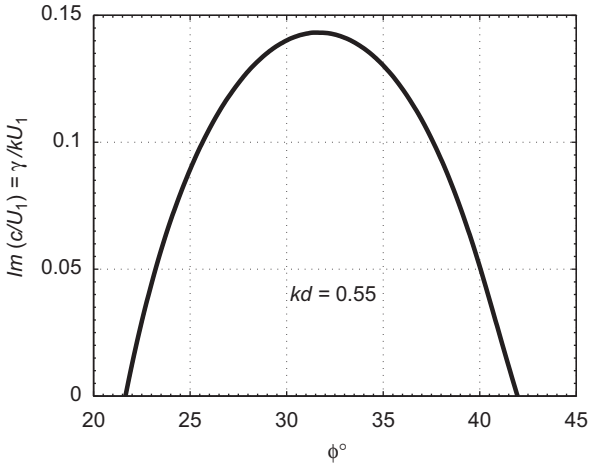

Fig. 10. Growth rate as a function of ϕ (angle of **k**–vector with flow direction). The dimensionless wavenumber $kd = 0.55$ is fixed at a constant value. The curve represents a normalized growth rate $Im(c/U_1) = \gamma/kU_1$. The maximum growth rate is for $\phi = 32^\circ$, which minimizes magnetic shear. Modes that deviate from this value by $\sim \pm 10^\circ$ have negligible growth because the instability is reduced by magnetic tensions. The growing **k**–vectors are thus confined to a narrow angular interval around the optimal ϕ value.

covers only a small velocity difference. Conversely, for long wavelengths the solution extends far on both sides of the layer, while the energy flow provided by a finite velocity difference spreads over a large region. This explains the decrease of γ as $k \to 0$.

Fig. 10 illustrates how the growth rate depends on the ϕ angle The dimensionless wavenumber $kd = 0.55$ is fixed at the constant value that maximizes the growth for the most favorable angle. The curve represents a normalized growth rate $Im(c/U_1) = \gamma/kU_1$. The maximum growth rate is for $\phi = 32^\circ$, which minimizes the magnetic shear. Modes that deviate from this value by $\sim \pm 10^\circ$

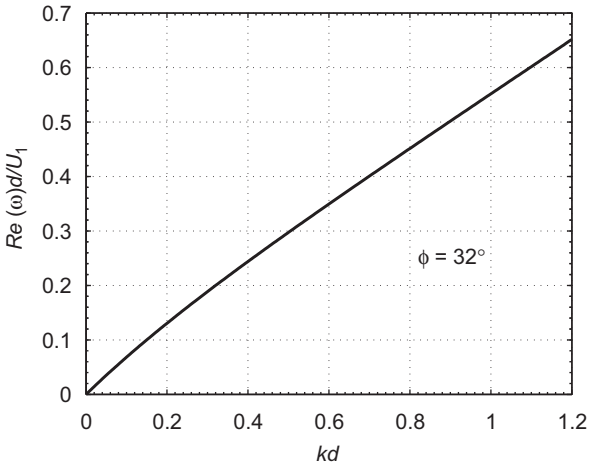

Fig. 11. The real part of the dispersion relation. Normalized real frequency $Re(\omega)d/U_1$ as a function of dimensionless wavenumber kd. The plot is for constant $\phi = 32^\circ$ (see captions of the previous figures). The normalized phase velocity $Re(\omega)/kU_1$ is nearly a constant. A wave packet around $kd = 0.55$ (which has the maximum growth rate) travels with the phase velocity and little spread (regarding angular dependence see Fig. 11). When the growth rate is maximum, $Re(\omega)/kU_1 = 0.59$, and the group velocity is $\approx (6/10)U_1$.

have negligible growth because the instability is reduced by the increasing magnetic tensions. Thus the fast growing **k**−vectors are confined to a narrow angular interval around the optimal ϕ value.

Fig. 11 displays the real part of the dispersion relation. The normalized real frequency $Re(\omega)d/U_1$ is plotted as a function of the dimensionless wavenumber kd. The plot is for constant $\phi = 32^\circ$. The normalized phase velocity $Re(\omega)/kU_1$ is nearly constant. A wave packet around $kd = 0.55$ (which has the maximum growth rate) travels with the phase velocity and little spread. For the angular dependence, see the remark on Fig. 10. When the growth rate reaches a maximum, $Re(\omega)/kU_1 = 0.59$, and the group velocity is $\approx (6/10)U_1$. Hence, from the measured frequency of the wavy perturbations we may derive an estimate of $k = 2\pi/\lambda$. Assuming we are observing the fastest growing perturbations, for which theory gives $kd = 0.55$, we can obtain an estimate of the boundary layer thickness $\Delta = 2d$. The result is $\sim 0.9\ R_E$, a value reported also in other studies of the near equatorial flanks.

4.3. KH instability: aspects of the non-linear theory

Undulatory perturbations appear soon after the large oscillations of the boundary and the concomitant clock angle decreases. The linear e-folding time, estimated as ~ 90 s, is too long to support an evolution of the instability starting from local noise. If the wave-like fluctuations observed by Cluster are of KH origin, we must hypothesize that the large oscillations have shortened the time needed for the non-linear features of the instability to appear. We assume that the spectrum of modes of the intense perturbation of the MP contains unstable modes with significant amplitude already at the start.

To examine the properties of the KH excitation in an advanced stage, and to test the hypothesis of shortened development of the process, we performed simulations of the non-linear dynamics, solving numerically the MHD equations for a local MP model. In large eddy simulations (LES) such as those we carried out, ideal MHD equations (inviscid and non-resistive) are sufficient to reveal the basic features of the vortices that the KH mechanism produces.

A numerical 3D+t code of the finite volume and arbitrary Lagrangian–Eulerian (FVALE) class was developed for this investigation by Bilbao (2006). It is designed to study LES for planar stratified models of the MP, with input parameters derived from spacecraft data. It solves the ideal, compressible MHD equations. The finite volume technique, which is different from the finite element method, relies on the integral version of the MHD equations. In general, the picture is a mix of Eulerian and Lagrangian descriptions chosen by computing efficiency criteria, and gives the "ALE" part of the name. The FV part comes from the conservative form of the MHD equations written for finite volumes.

The computational box is subdivided into discrete 3D cells of arbitrary shape, which may change during the time evolution. The code carries out the bookkeeping of temporal variations of MHD field quantities in each cell. Mean values of adjacent cells allow the interpolation of values to the common surfaces of the cells. Conversely, with the surface values of each cell, the mean value over the cell can be computed. Finally, some cell surfaces touch the boundaries of the computing box, and there boundary values are introduced. The code checks the global conservation in time of sensitive physical quantities. The computation controls, for instance, that $\mathrm{div}\,\mathbf{B} = 0$ is satisfied within a given numerical tolerance. We omit for brevity other technical details of the technique, and the code, that the reader may find in Bilbao (2006) and Gratton et al. (2009).

For the numerical simulation the initial structure of the LLBL uses the same model we employed as a starting point for the linear stability analysis, i.e. a combined vortex and current layer. In the numerical runs of the code the initial perturbation was given as a variation of the velocity field at 10% amplitude with respect to the laminar background flow, with the features of a fast growing mode. The initial perturbation was oriented at $\varphi = 32^\circ$ with respect to the main flow set along the X axis, as predicted for the most unstable modes by linear analysis. The intense perturbation of the MP was assumed to comprise unstable modes with significant magnitudes. In the reported examples, we use periodic boundary conditions in X and Z, while on the two computing boundaries normal to the Y axis, the field quantities are fixed at values corresponding to the magnetosheath ($Y > 0$) and the magnetosphere ($Y < 0$), respectively. In our simulation runs, which study about 180 s of model real time, the discretization resolution was set at $56 \times 40 \times 88 = 197,120$ cells.

During the simulation some streamlines are observed to oscillate strongly, meandering in and out of the magnetosphere. Some streamlines that start in regions of intermediate velocity and density, later on deviate conspicuously, passing through magnetospheric regions with minimal speed. This is indicative of long permanence times of higher-density plasma elements in low density regions, near the inner boundary of the MP.

The growth time for the appearance of salient non-linear features turns out to be comparable with the linear e-folding time τ_e when the model starts from a noticeable perturbed state that contains unstable modes. To designate this shortened build-up of vortices in the boundary layer, we devised the simplified expression "acceleration of the instability".

We mention here briefly some results closely related to the observational and theoretical discussions of this paper. In Fig. 12 we show the build-up of large vortices from a CS/VS initial stage by the KH process. The result is from a numerical LES with input data tailored to the December 7, 2000 boundary layer conditions. The 3D figure is for a $t = 89$ s after the initial perturbation, which is about $\frac{1}{2}\tau_r$ the vortex roll-over time; $\tau_r = 2d/U_1$ is a typical time scale for plasma rotation around the core. The local axes of the figure are in units of R_E; X horizontal right (antisunward, parallel to the flow), Y horizontal left (across the boundary layer), Z

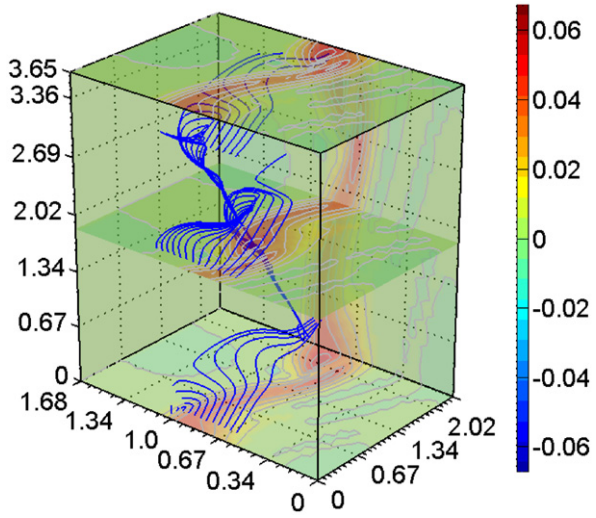

Fig. 12. KH build-up of large vortices from a TD-VS initial stage. Result from a numerical LES with input data tailored to December 7, 2000 boundary layer configuration (see text). The 3D figure is for a $t=89$ s after the initial perturbation, about $\frac{1}{2}\tau_r$ roll-over time. Local axes are in units of the Earth radius R_E; X horizontal right (antisunward, parallel to the flow), Y horizontal left (across the boundary layer), Z vertical. The color scale indicates ω, the vorticity strength (in 1/s units) where $\omega=|\mathrm{curl}(\mathbf{v})|\ \mathrm{sign}(\omega_z)$ $(s|\omega=\mathrm{curl}(\mathbf{v}))$. The contour planes illustrate the concentration of vorticity into vortex cores, with increase of intensity with respect to the maximum initial value ($\omega_i\sim0.049$). The blue curves are a set of streamlines that indicate the formation of swirling flows in the vortex cores. The simulation illustrates the acceleration of the KH evolution when the system is subject to a significant initial perturbation (here $\sim10\%$ of the unperturbed flow speed), which triggers the instability, and stimulate large effects on times comparable with the e-folding time $\tau=1/\gamma$ (roughly ~90 s, depending on estimates of the thickness of the layer). (For interpretation of the references to color in this figure legend, the reader is referred to the web version of this article.)

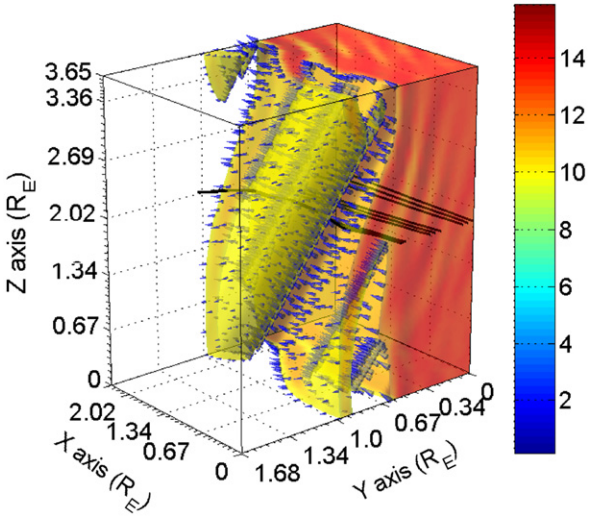

Fig. 13. Turn-over of a large vortex and concomitant density mixing (from a numerical LES for December 7, 2000). The plot is for $t=180$ s after the initial perturbation, $\sim\tau_r$ one roll-over time. The 3D figure shows the isodensity surface for $n=9$ p/cm^3, an intermediate value between magnetosheath and magnetospheric levels. The color scale indicates particle density in p/cm^3. Axes are similar to Fig. 13, but with X horizontal left and Y horizontal right, to exhibit better the equal density surface. The blue cones indicate the local direction and relative strength of the velocity field. A few stream lines are shown in black. The figure illustrates the fact that large-amplitude changes of the boundary layer, generated by the KH mechanism, may be expected on time scales comparable to the theoretical growth rate after the action of a strong trigger. (For interpretation of the references to color in this figure legend, the reader is referred to the web version of this article.)

vertical. The color scale indicates ω, the vorticity strength (in units of 1/s) where $\boldsymbol{\omega}=|\mathrm{curl}(\mathbf{v})|\mathrm{sign}(\omega_z)(s|\omega=\mathrm{curl}(\mathbf{v}))$. The contour planes illustrate the concentration of vorticity into vortex cores, with increase of intensity with respect to the maximum initial value ($\omega_i\sim0.049$). The blue curves represent a set of streamlines that indicate the formation of swirling flows in the vortex cores. The simulation illustrates the speeding-up of KH evolution when the system is subject to a significant initial perturbation (that was set at $\sim10\%$ the unperturbed flow speed), which triggers the instability, and stimulate large effects on time scales comparable with the e-folding time $\tau=1/\gamma$ roughly ~90 s, depending on the estimate of the thickness of the layer.

The roll-over of a large vortex is shown in Fig. 13. The plot is for $t=180$ s after the initial perturbation, $\sim\tau_r$ one turn-over time. The figure shows the isodensity surface for $n=9\,\mathrm{cm}^{-3}$, intermediate between magnetosheath ($2.3\,\mathrm{cm}^{-3}$) and magnetospheric ($13.6\,\mathrm{cm}^{-3}$ values. The color scale indicates the plasma density in cm^{-3}. Axes are similar to Fig. 12, but with X horizontal left and Y horizontal right to better show the isodensity surface. The blue cones indicate the local direction and the relative strength of the velocity field. A few streamlines in black are also drawn. The result again underlines the fact that large–amplitude changes of the boundary layer, generated by the KH mechanism, may be expected on times comparable to the theoretical growth rate, after the action of a strong trigger.

5. Discussion and conclusions

Sudden changes in the solar wind flow parameters and/or interplanetary magnetic field have been the subject of many studies, both from an interplanetary point of view (their nature, frequency of occurrence, etc.) as well as for the effects they cause in the magnetosphere. In this article on effects of discontinuities on the magnetosphere and the role of KH-driven MP surface waves, we concentrated on an interplanetary structure which included both: A CS which was simultaneously a VS, and which introduced a period of strongly northward IMF orientation. We showed that the VS aspect of the first trigger was crucial for magnetopheric dynamics in that changes in the tangential stresses were by a factor of three larger than the normal (dynamic) pressure. The response was monitored by Cluster, which was crossing the duskside MP. Three-minute period oscillations were set up by the first trigger in which the MP boundary oscillated at large amplitude over the spacecraft, causing it to sample alternately the cold/dense plasma of the magnetosheath and the hot/tenuous plasma of the magnetosphere. These in turn provided us with input magnetosphere/magnetosheath quantities needed for our linear perturbation analysis of the MHD equations to address the response to the period of northward IMF. We found that the duskside MP was KH-unstable, with waves of ~79 s period being generated.

The effect of the first trigger was not just a local one. Studying ground magnetometer records from stations spanning about 12 h in local time, we found that oscillatory signals were excited there within certain latitude bands. Further, the presence of resonating L-shells could be ascertained from the peaking of the amplitude at certain latitudes in a meridional station chain and the phase reversal between neighboring stations. Thus the effect of tangential stresses applied to the MP is a global one and the dynamics of the magnetosphere are driven from its boundary.

In many ways the response is similar to that excited by a large, dynamic pressure change such as modeled by Southwood and Kivelson (1990) and observed by Farrugia et al. (1989) and Sibeck (1990). Strong resonant modes are excited in both cases. We do

not believe that we are dealing with a global change in the geomagnetic field. We think that the oscillatory motion of the boundary seen at Cluster does not originate from global body motion, or windsock-type shifts of the whole magnetosphere.

How did the disturbance travel to the Cluster location from the point of impact? Two possibilities suggest themselves: the tangential stresses generated large "wrinkles" in the MP surface which were then carried either by (i) convection, as the CS/VS folds over and around the MP boundary; or (ii) by propagation as large-amplitude surface waves. In view of the small time delay between the response at Cluster and that on the ground magnetometers, we favor the former hypothesis.

It is interesting to note that examining 1 min resolution plasma data from the IMP 8 spacecraft, which at 14 UT was located at $(4.26, -31.42, 4.16)$ R_E, i.e. on the dawnside and north of the ecliptic, we do not find evidence of sudden flow rotations. This indicates that the DD has a limited extent in the plane transverse to the Sun Earth line. Fortuitously, it reached Wind (located at $(36, 178, -8)$ R_E at 12 UT), ACE, and the Earth, but not IMP-8.

The work emphasized the role in exciting important mageto-pause/magnetosphere motions of the azimuthal component of the solar wind velocity, a quantity which is usually given scant attention. Recently, Zong et al. (2004) illustrated the ability of a steep change in this component to cause large motions of the cusp. Here we illustrated another aspect of its effects. As an aside, one might note that interplanetary situations where the non-radial components of the solar wind velocity may be expected to be significant occur when the leading edge of ICMEs or magnetic clouds pass earth. This is because the solar wind tries to flow around the ICME boundary in the sheath, so that the direction of the solar wind close to the ICME boundary ought to be significantly different from radial. Thus, studying a planar structure in the inner sheath of an ICME on November 20, 2003, Farrugia et al. (2008b) find rotations in the east–west and north–south components of the solar wind velocity comparable to those here, although more spread out in time (see their Fig. 3).

The interplanetary structure whose effect on the magneto-sphere we examined was particularly well suited for this task. For example, the east–west rotation of the magnetic field, ΔB_y, and bulk plasma velocity, ΔV_y, occurred at essentially constant total field and bulk flow speed.

In our work we have ignored the interaction of the CS/VS with the bow shock. Our justification for doing so is as follows. As the simulations by Wu et al. (1993) show, the interaction depends mainly on the density change across the discontinuity. Here there was merely $\sim 9\%$ change. Further, the passage at constant B helps to make this interaction even weaker. The changes of interest to us were tangential to the discontinuity which are unaffected by the bow shock. Thus we were able to sidestep complications which this interaction normally brings, in the form of subsidiary MHD wave modes on which the initial density change is distributed and which travel at different speeds in the magnetosheath, exposing the magnetosphere to a succession of effects.

From the theoretical analysis we emphasize the following point. As observed in situ by Cluster, close to the moment the high-frequency perturbations are recorded the magnetic shear becomes very small. Not surprisingly, therefore, the most unstable KH mode has its $\mathbf{k}$−vector roughly perpendicular to the average magnetosheath and magnetosphere field directions, so that it characterizes flute modes with $\mathbf{B}\cdot\mathbf{k}\approx 0$. As noted, a change in the $\mathbf{k}$−direction of $\pm 10^{\circ}$ is sufficient to stabilize the configuration. The fast growing modes all have on the MP surface wave vectors oriented in a small angular interval around the $+32^{\circ}$ direction with respect to the main flow. A larger amount of magnetic shear, as was indicated by the clock angle of the IMF before the discontinuity arrival, inhibits the instability at the Cluster locale, and even more so at upstream MP sites, where the Alfvén Mach number is smaller, and the magnetic tensions stronger. The observed experimental fact that the high-frequency waves appear soon after the large-amplitude oscillations of the boundary leads us to conclude that the intense MP perturbations shortened the appearance of the non-linear phase of the KH instability. In other words, the impact of the CS/VS on the magnetosphere triggered a fast progress of the KH mechanism, rolling over the vorticity layer. It is not a matter of a rise from a small level of noise over many e-folding times. Rather, it is a precipitous take-off of the instability from an already intensely perturbed flow. From the analysis the maximum growth rate is for a wavelength $\approx 5.7\Delta$. With an estimated boundary layer thickness $\sim 0.9R_E$ the e-folding time of the linear stage is then $\tau = 1/\gamma \sim 90$ s. The numerical LES we have commented upon in Section 4.3 confirm that the build-up of large vortices in the boundary layer takes place in about one turnover time, which is comparable to the e-folding time, when the numerical experiment starts from a significant perturbation of the velocity field. This is what we have, for short, called "the speeding up of the instability".

To conclude, we have shown that changes in the azimuthal velocity of the solar wind occurring at a discontinuity and the ensuing period of northward IMF excited large motions at the MP and the magnetosphere over a wide spread of magnetic local times. Large deformations of the surface gave way to higher frequency signals driven by the KH instability. The non-linear development was apparently speeded by the previous perturbations, and large vortical structures were formed.

Acknowledgments

We thank JGR for permission to use Fig. 6 from Farrugia et al. (2008a). We are grateful to our coworkers L. Bilbao and G. Gnavi (from INFIP, CONICET, UBA) for their help with some theory figures, and to Eric J. Lund and Bernie Vasquez for helpful discussions. We also thank NOAA for the GOES 8 data. C.J. Farrugia is supported by NASA Grants NNX08AD11G, NNG05GG25G and Cluster grant to UNH. F.T. Gratton is supported by CONICET Grant PIP 5291, and UBA research Grant CYT X90.

References

Balogh, A., et al., 1997. The Cluster magnetic field investigation. Space Sci. Rev. 79, 65.

Belmont, G., Chanteur, G., 1989. Advances in magnetopause Kelvin–Helmholtz instability studies. Phys. Scr. 124, 124.

Bilbao, L.E. 2006. A three-dimensional finite volume arbitrary Lagrangian–Eulerian code for plasma simulations. In: Herrera Vazquez, J.J.E. (Ed.), American Institute of Physics Conference Proceedings on Plasma and Fusion Science, vol. 875, p. 467.

Cable, S., Lin, Y., 1998. Three-dimensional MHD simulations of interplanetary rotational discontinuities impacting the Earth's bow shock and magnetosheath. J. Geophys. Res. 103 (A12), 29,551–29,567.

Dungey, J.W., 1954. Electrodynamics of the outer atmosphere, Pennsylvania State University Ionosphere Research Laboratory Science Report, No. 69.

Fairfield, D.H., Farrugia, C.J., Mukai, T., Nagai, T., Fedorov, A., 2003. Motion of the dusk flank boundary layer caused by solar wind pressure changes and the Kelvin–Helmholtz instability: January 10–11, 1997. J. Geophys. Res. 108 (A12), 1460 10.1029/2003JA010134.

Farrugia, C.J., Gratton, F.T., Torbert, R.B., 2001. The role of viscous-type processes in solar wind-magnetosphere interactions, in challenges to long-standing unsolved problems in space physics in the 20th century. Space Sci. Rev. 95, 443.

Farrugia, C.J., Freeman, M.P., Cowley, S.W.H., Southwood, D.J., Lockwood, M., Etemadi, A., 1989. Pressure-driven magnetopause oscillations and attendant response on the ground. Planet. Space Sci. 37, 589.

Farrugia, C.J., Gratton, F.T., Bender, L., Biernat, H.K., Erkaev, N.V., Denisenko, V., Torbert, R.B., Quinn, J.M., 1998. J. Geophys. Res. 103, 6703.

Farrugia, C.J., Gratton, F.T., Lund, E.J., Sandholt, P.E., Cowley, S.W.H., Torbert, R.B., Gnavi, G., Mann, I.R., Bilbao, L., Mouikis, C., Kistler, L., Smith, C.W., Singer, H.J., Watermann, J.F., 2008a. Two-stage oscillatory response of the magnetopause

to a tangential discontinuity/vortex sheet followed by northward IMF: Cluster observations. J. Geophys. Res. 113, A03208 10.1029/2007JA012800.
Farrugia, C.J., Erkaev, N.V., Taubenschuss, U., Shaidurov, V.A., Smith, C.W., Biernat, H.K., 2008b. A slow mode transition region adjoining the front boundary of a magnetic cloud as a relic of a convected solar wind feature: observations and MHD simulation. J. Geophys. Res. 113, A00B01 10.1029/2007JA012953.
Freeman, M.P., Farrugia, C.J., Cowley, S.W.H., Southwood, D.J., Lockwood, M., Etemadi, A., 1990. The response of the magnetosphere–ionosphere system to solar wind dynamic pressure variations. In: Russell, C.T., Priest, E.R., Lee, L.C. (Eds.), Physics of Magnetic Flux Ropes, vol. 611, Geophysical Monograph 58, AGU.
Friis-Christensen, E., McHenry, M.A., Clauer, C.R., Vennerstrom, S., 1987. Ionospheric traveling convection vortices observed near the polar cleft: a triggered response to sudden changes in the solar wind. Geophys. Res. Lett. 15, 253–256.
González, A.G., Gratton, J., 1994a. J. Plasma Phys. 51, 43–60.
González, A.G, Gratton, J., 1994b. J. Plasma Phys. 52, 223–244.
Gratton, F.T., Bender, L., Farrugia, C.J., Gnavi, G., 2004. J. Geophys. Res. 109, doi: 10.102V2003JA010146.
Gratton, F.T., Gnavi, G., Farrugia, C.J., Bender, L., 2005. On the MHD boundary of Kelvin-Helmholtz stability diagram at large wavelenghts. Braz. J. Phys. 34 (4B), 1804.
Gratton, F.T., Bilbao, L., Farrugia, C.J., Gnavi, G., 2009. Large eddy simulations of counter-rotating vortices at the magnetopause. J. Phys. CS 166, doi: 10.1088/1742-6596/166/1/102023.
Gratton, J.A., González, G., Gratton, F.T., 1988. Convective instability of internal modes in accelerated compressible plasmas. Plasma Phys. Controlled Fusion 30, 435.
Keller, H.B., 1992. Numerical Methods for Two Point Boundary-Value Problems. Dover, NY.
Kivelson, M.G., Chen, S.-H., 1995. The magnetopause: surface waves and instabilities and their possible dynamical consequences. In: Song, P., Sonnerup, B.U.O., Thomsen, M.F. (Eds.), Physics of the Magnetopause, Geophysics Monograph Series, vol. 90, AGU, Washington, DC, p. 257.
Lin, Y., Swift, D.W., Lee, L.C., 1996a. Simulation of pressure pulses in the bow shock and magnetosheath driven by variations in interplanetary magnetic field direction. J. Geophys. Res. 101 (A12), 27,25127.
Lin, Y., Lee, L.C., Yan, M., 1996b. Generation of dynamic pressure pulses downstream of the bow shock by variations in the interplanetary magnetic field orientation. J. Geophys. Res. 101 (A1), 479.
Lin, Y., 1997. Generation of anomalous flows near the bow shock by its interaction with interplanetary discontinuities. J. Geophys. Res. 102 (A11), 24,265.
Lundin, R., Aparcio, B., Yamauchi, M., 2001. On the solar wind flow control of the polar cusp. J. Geophys. Res. 106 (A7), 13,023.
Maynard, N.C., Farrugia, C.J., Ober, D.M., Burke, W.K., et al., 2008. Cluster observations of fast shocks in the magnetosheath launched as a tangential discontinuity with a pressure increase crossed the bow shock. J. Geophys. Res., 113, A10212, doi: 10.1029/2008JA013121.
McComas, D.J., et al., 1998. Solar wind electron, proton, and alpha monitor (SWEPAM) for the advanced composition explorer. Space Sci. Rev. 86, 563.
McHenry, M., Clauer, C., 1987. Modeled ground magnetic signatures of flux transfer events. J. Geophys. Res. 92 (A10), 11231–11240.
McHenry, M., Clauer, C., 1989. Correction to "Modeled ground magnetic signatures of flux transfer events". J. Geophys. Res. 94 (A10), 13601.
Miura, A., 1990. Kelvin–Helmholtz instability for supersonic shear flow at the magnetospheric boundary. Geophys. Res. Lett. 17, 749.
Miura, A., 1984. Anomalous transport by magnetohydrodynamic Kelvin–Helmholtz instabilities in the solar wind–magnetosphere interaction. J. Geophys. Res. 89 (A2), 801.
Miura, A., 1987. Simulation of Kelvin–Helmholtz instability at the magnetospheric boundary. J. Geophys. Res. 92 (A4), 3195.
Miura, A., 1992. Kelvin-Helmholtz instability at the magnetospheric boundary, Dependence on the magnetosheath sonic Mach number. J. Geophys. Res. 97, 10,655.
Rème, H., et al., 1997. The cluster ion spectrometry (CIS) experiment. Space Sci. Rev. 7 (1–2), 303.
Russell, C.T., Elphic, R.C., 1978. Initial ISEE magnetometer results: magnetopause observations. Space Sci. Rev. 22, 681.
Saunders, M.A., Russell, C.T., Sckopke, N., 1984. Flux transfer events: scale size and interior structure. Geophys. Res. Lett. 11 (2), 131.
Shue, J.-H., et al., 1998. Magnetopause location under extreme solar wind conditions. J. Geophys. Res. 103 (A8), 17,691.
Sibeck, D.G., 1990. A model for the transient magnetospheric response to sudden solar wind dynamic pressure variations. J. Geophys. Res. 95, 3755.
Smith, C.W., et al., 1998. The ACE magnetic fields experiment. Space Sci. Rev. 86, 613.
Sonnerup, B.U.O., Cahill Jr., L.J., 1967. Magnetopause structure and attitude from Explorer 12 observations. J. Geophys. Res. 72, 171.
Southwood, D.J., 1987. The ionospheric signatures of flux transfer events. J. Geophys. Res. 92, 3207.
Southwood, D.J., Kivelson, M.G., 1990. The magnetohydrodynamic response of the magnetospheric cavity to changes in solar wind pressure. J. Geophys. Res. 95 (A3), 2301.
Vasquez, B.J., Abramenko, V.I., Haggerty, D.K., Smith, C.W., 2007. Numerous small magnetic field discontinuities of Bartels rotation 2286 and the potential role of Alfvénic turbulence. J. Geophys. Res. 112 doi:10.1029/2007JA0112504.
Wu, B.H., Mandt, M.E., Lee, L.C., Chao, J.K., 1993. Magnetospheric response to solar wind dynamic pressure variations: interaction of interplanetary tangential discontinuities with the bow shock. J. Geophys. Res. 98 (A12), 21,297.
Zong, Q.-G., Fritz, T.A., Zhang, H., Korth, A., Daly, P.W., Dunlop, M.W., Glassmeier, K.-H., Reme, H., Balogh, A., 2004. Triple cusps observed by Cluster—temporal or spatial effect? Geophys. Res. Lett. 31, L09810, doi: 10.1029/2003GL019128.